

Cryo-EM characterization of the anhydromuropeptide permease AmpG central to bacterial fitness and β -lactam antibiotic resistance

Sverak HE¹, Yaeger LN², Worrall LJ^{1, 3}, Vacariu CM⁴, Glenwright AJ¹, Vuckovic M¹, Al Azawi ZD², Lamers RP², Marko VA², Skorupski C², Soni AS⁴, Tanner ME⁴, Burrows LL², Strynadka NCJ^{1, 3*}

¹Department of Biochemistry and Molecular Biology and the Center for Blood Research, University of British Columbia, Vancouver, BC, Canada.

²Department of Biochemistry and Biomedical Sciences and the Michael G. DeGroot Institute of Infectious Disease Research, McMaster University, Hamilton, Ontario, Canada.

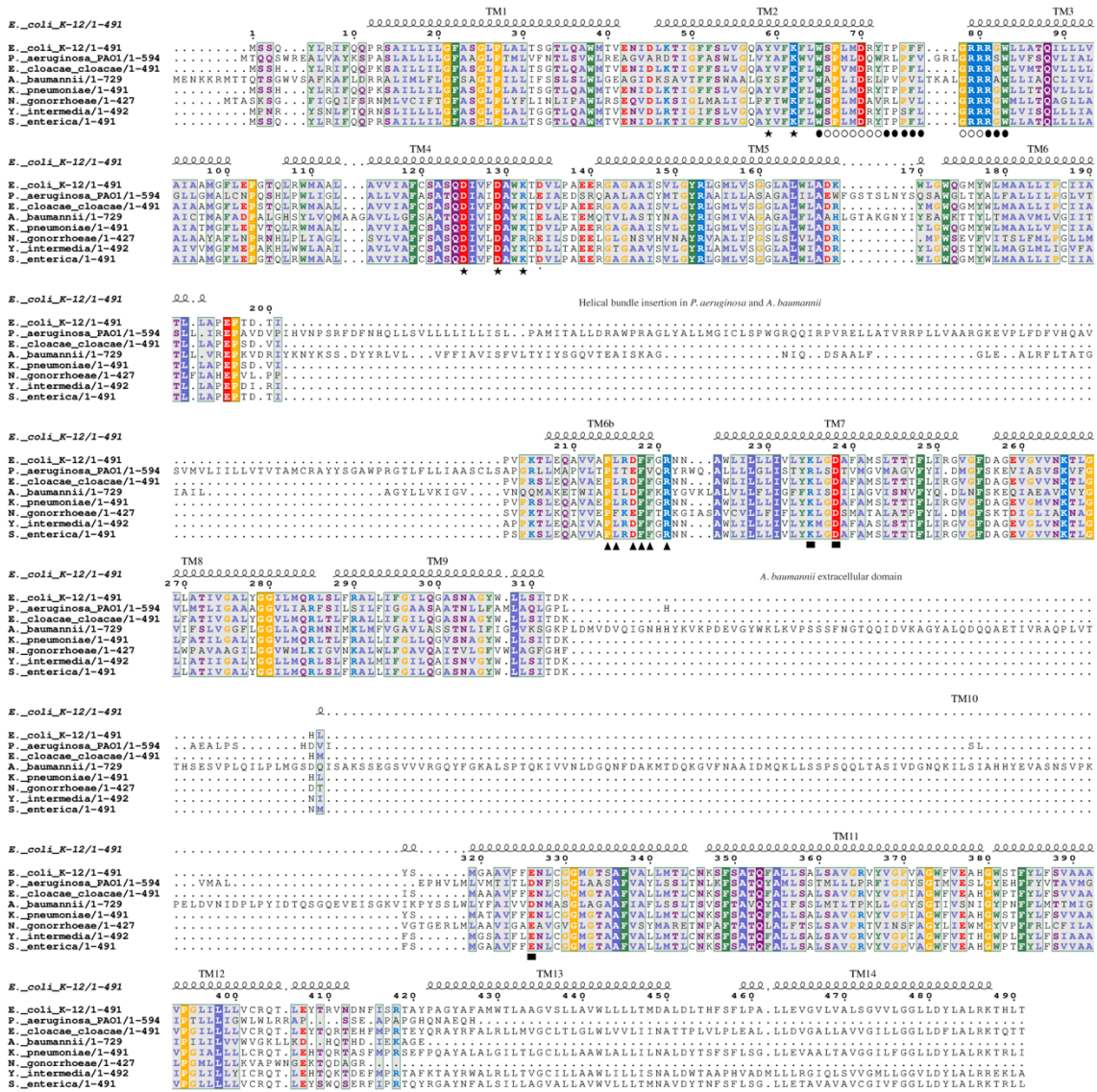
³High Resolution Macromolecular Cryo-Electron Microscopy (HRMEM) Facility, University of British Columbia, Vancouver, BC, Canada.

⁴Department of Chemistry, University of British Columbia, Vancouver, BC, Canada.

This file contains Supplementary Table 1-2, Supplementary Figures 1-11, and Supplementary Methods

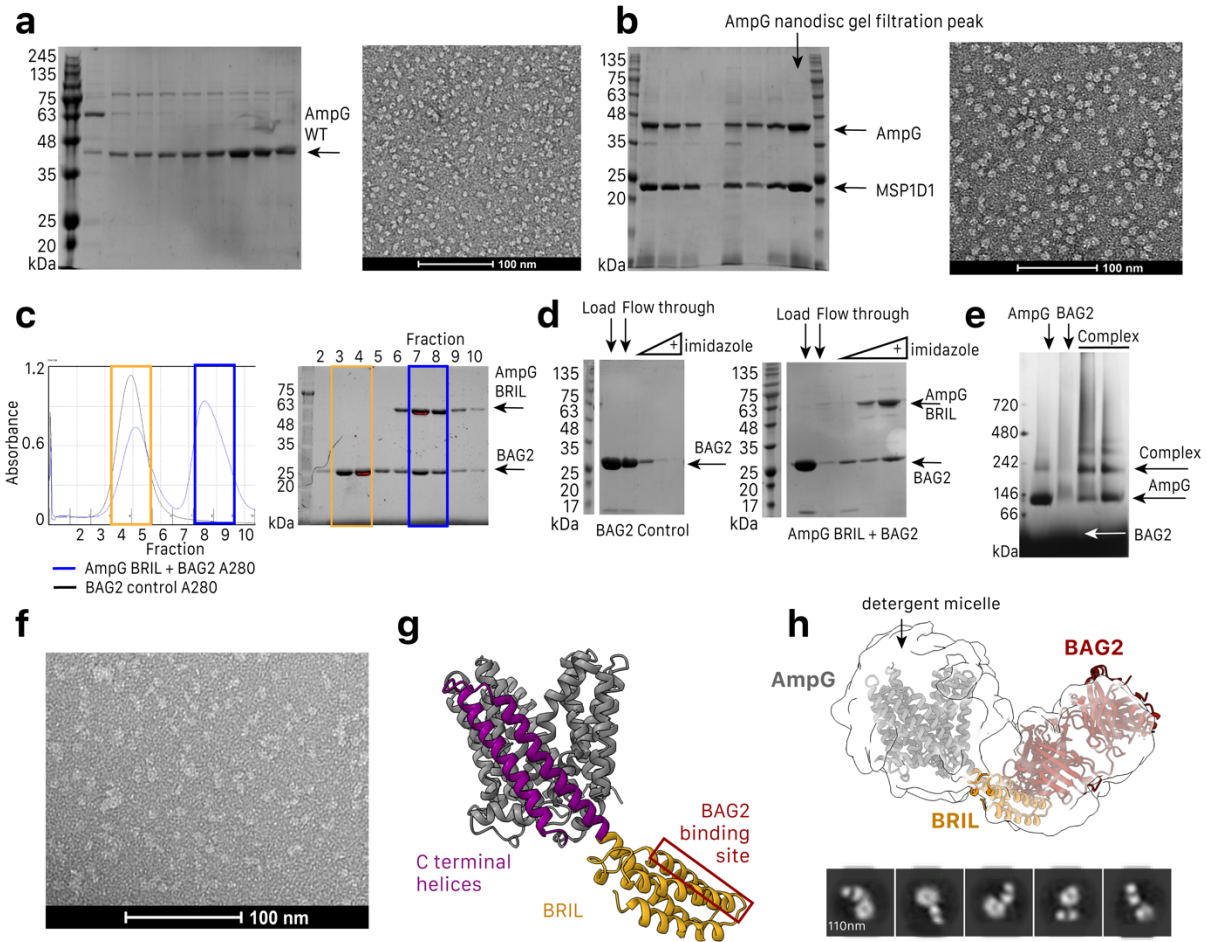
AmpG WT	
EMD-28658 / PDB 8EXP	
Data collection and processing	
Microscope	TF Titan Krios
Camera	Falcon 4i
Voltage (kV)	300
Magnification	
Defocus range (μm)	0.5 to 3.0
Movies	43,215
Pixel size (\AA)	0.59
Total dose ($e^-/\text{\AA}^2$)	50
Symmetry imposed	C1
Particles initial / final	5,216,322 / 503,623
Map resolution (\AA)	3.8
FSC threshold	0.143
Map resolution range	2.55-5.14
Model refinements	
Initial model used (PDB code)	de novo
Model resolution (\AA)	3.8
FSC threshold	0.143
Map-to-model cross-correlation	0.73
Map sharpening B factor (\AA^2)	-240
Model composition	
Nonhydrogen atoms	3749
Protein	3714
Ligands	35
Mean model B factors (\AA^2)	
Protein	159.4
Ligands	173.4
R.m.s. deviations	
Bond lengths (\AA)	0.007
Bond angles ($^\circ$)	1.57
Validation	
MolProbity score	1.05
All-atom clashscore	2.62
Rotamer outliers (%)	0.00
C-beta deviations	0.45
Ramachandran plot	
Favoured (%)	98.14
Allowed (%)	1.86
Disallowed (%)	0.00

Supplementary Table 1: *E. coli* AmpG cryo-EM data processing.

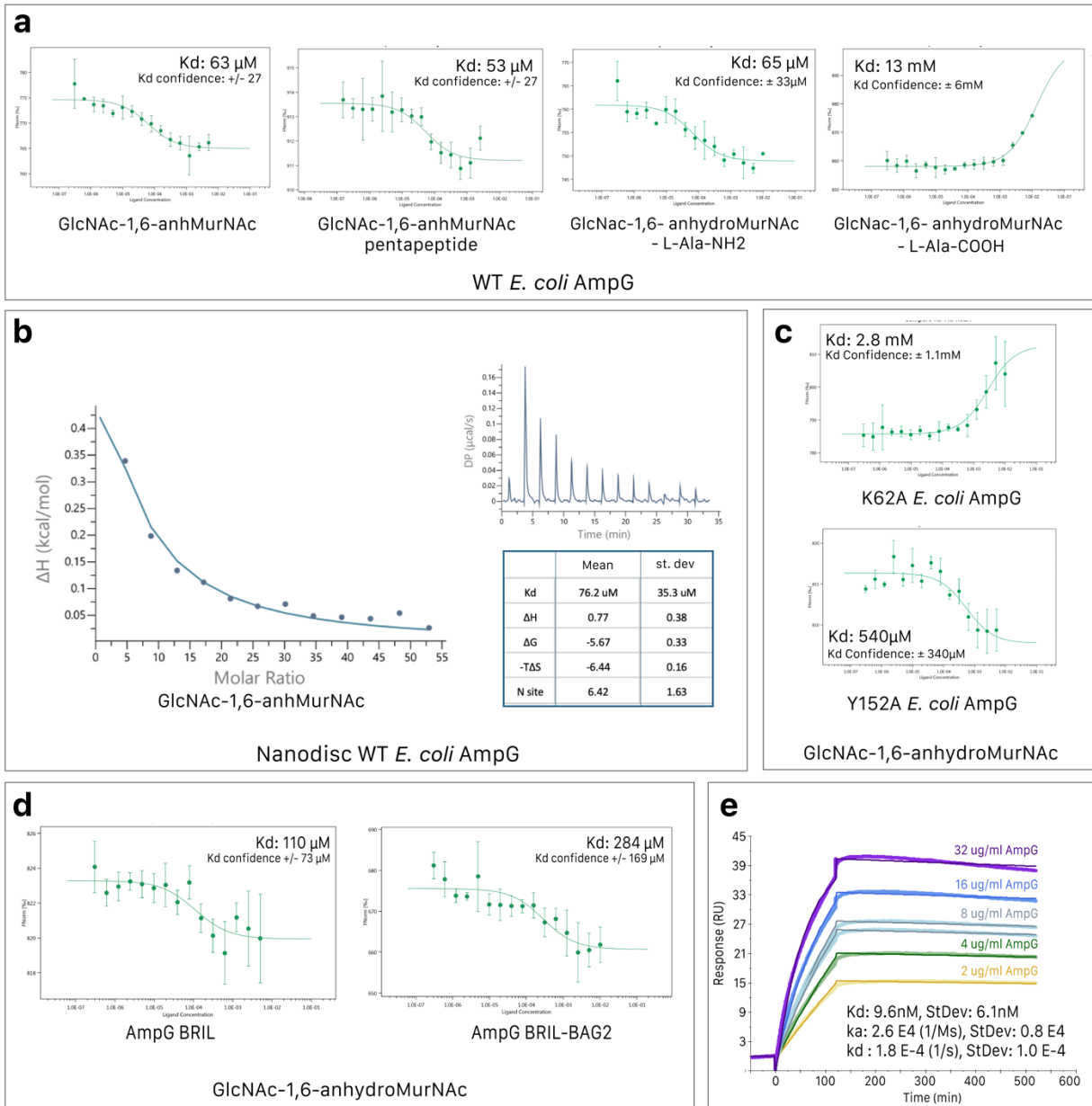


★ N-terminal AmpG cluster ○ canonical motif A ● AmpG specific motif A ▲ AmpG wedge ■ C-terminal AmpG cluster

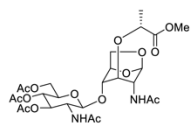
Supplementary Fig. 1: Sequence alignment¹ of AmpG homologs from various strains of clinical significance. Alignment with homologs of AmpG in *E. coli* MG1655:EG12183, *P. aeruginosa* (GCF_000006765.1):PA4393, *E. cloacae* ATCC_13047:ECL_01191, *A. baumannii* 3909:AB3909_RS0108355, *K. pneumoniae* HS11286:KPHS_11350, *N. gonorrhoeae* FQ02:EGH17_RS09275, *Y. intermedia* NCTC11469:EL015_RS16020, and *S. enterica* K6L45_RS19750 obtained by NCBI last².



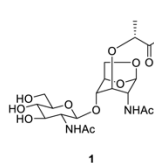
Supplementary Fig. 2: *E. coli* AmpG protein characterization. **a**, SDS-PAGE and negative stain EM analysis of wild-type (WT) *E. coli* AmpG. AmpG migrates faster than expected for a ~53 kDa protein, which is not unusual for a membrane protein. **b**, as **a** for AmpG reconstituted with MSP1D1 (MW 23 kDa). **c**, Glycerol gradient ultracentrifugation and SDS-PAGE analysis of AmpG-BRIL (10 kDa larger than WT AmpG) and BAG2 Fab. **d**, Immobilized metal chromatography pull down of His-tagged AmpG with BAG2 compared to BAG2 control alone. **e**, Native PAGE of glutaraldehyde cross-linked samples of AmpG, BAG2, and complex. **f**, Negative stain EM of AmpG-BRIL BAG2 complex. **g**, AlphaFold3³ model (Predictive template modeling score = 0.77) of AmpG-BRIL, with BRIL shown in gold as a helical structure extended from the C-terminal helix (TM14) of AmpG (purple). **h**, Negative stain EM reconstruction of AmpG-BRIL BAG2. The AmpG-BRIL model and BAG2 crystal structure (PDB: 6CBV) are docked into the experimental map.

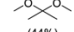


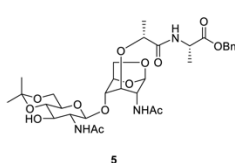
Supplementary Fig. 3: In vitro binding data for AmpG. **a**, Microscale thermophoresis (MST) of wild-type (WT) *E. Coli* AmpG solubilized in DDM binding to GlcNAc-1,6-anhydroMurNAc (1), with either a free carboxylate Ala-COOH (2), amidated Ala-NH2 (3) peptide R group, and GlcNAc-1,6-anhydroMurNAc-pentapeptide (4). Performed in triplicate, shown as average values with error bars showing standard deviation **b**, Binding of GlcNAc-1,6-anhydroMurNAc (1) to AmpG in MSP1D1 nanodiscs⁴ using ITC and performed in biological triplicate, with a representative trace shown. **c**, MST of *E. Coli* AmpG mutants solubilized in DDM with GlcNAc-1,6-anhydroMurNAc (1). Both mutants have lower binding than wild type, with K62A showing much weaker binding than Y152. **d**, MST of *E. Coli* AmpG BRIL and BAG2 complex to GlcNAc-1,6-anhydroMurNAc. **e**, Surface Plasmon Resonance (SPR) of AmpG interaction with BAG2 with a binding constant of 9.7nM. Experiment performed in biological triplicate, a representative run is shown.

a

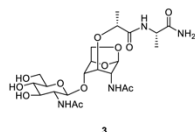
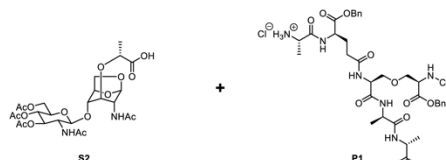
1) KOH, H₂O,
MeOH
2) Dowex-H, H₂O,
MeOH
(quant.)



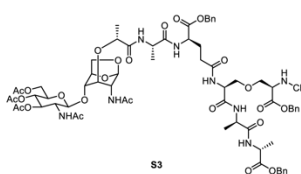
1)
Cl⁻
H₃N⁺ C(=O) OBn
PyBOP, HOBT,
DIPEA
2) HOTs·H₂O,
acetone,

(44%)



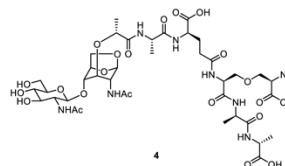
1) NH₃ in MeOH
2) Dowex-H, H₂O,
MeOH
(85%)

**b**

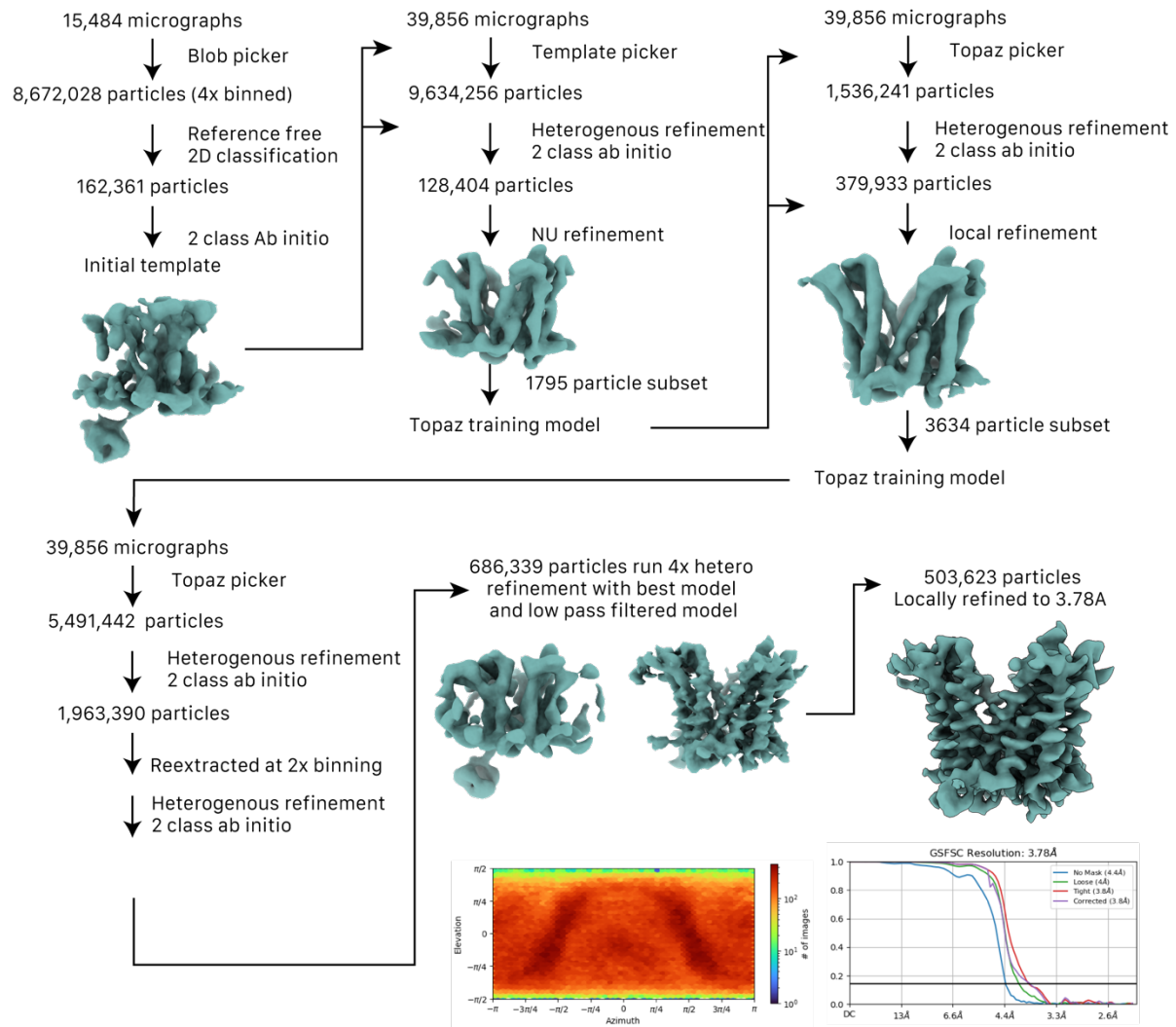
EDCI, HOBT,
DIPEA
(26%)



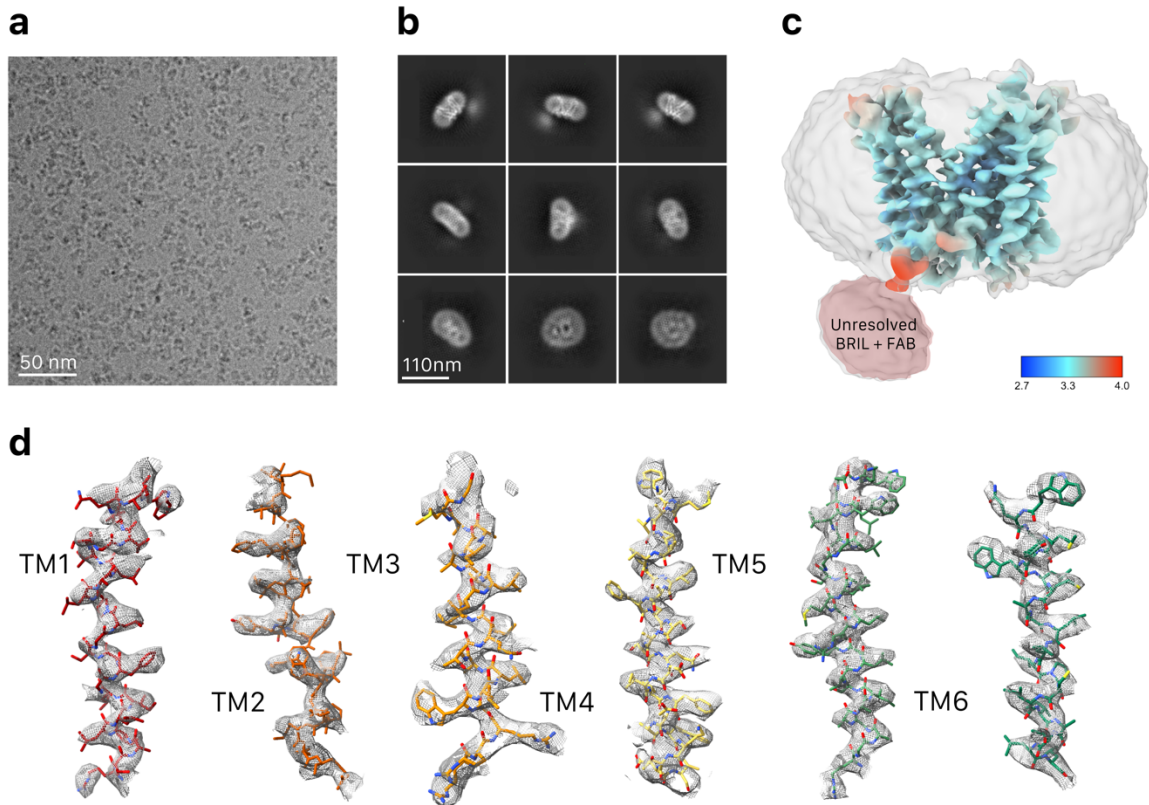
1) Pd/C, H₂(g)
2) K₂CO₃, H₂O,
MeOH
(62%)



Supplementary Fig. 4: Chemical synthesis of AmpG substrate analogs. a, Chemical synthesis of compounds **2** and **3** from the precursor compound, including novel L-alanine-bearing disaccharide **5** by a preliminary coupling reaction to L-alanine benzyl ester via PyBOP/HOBT and acetonide protection. **b**, Synthesis of GlcNAc-1,6-MurNAc-pentapeptide through separate chemical synthesis of meso-oxa-Dap.



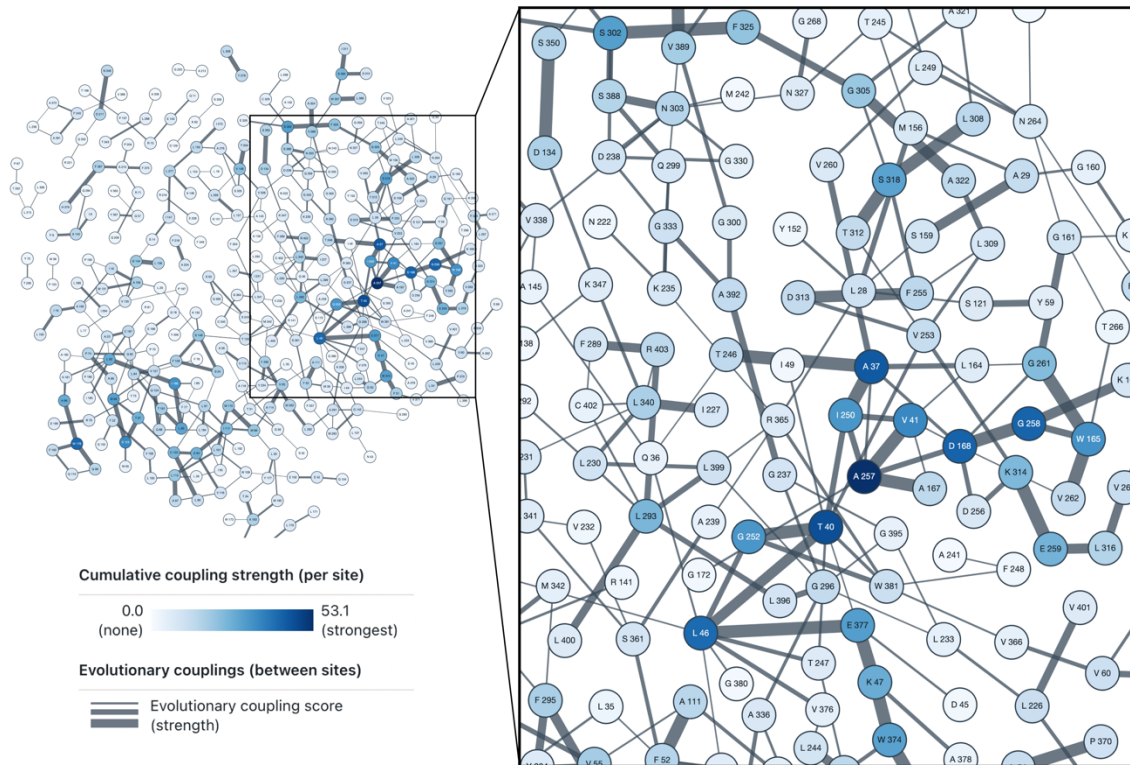
Supplementary Fig. 5: Cryo-EM processing workflow. Cryo-EM processing was performed using CryoSPARC version 4.4.1⁵. Multiple rounds of particle picking were necessary for improvements of resolution. Gold Standard Fourier Shell Correlation (GSFSC) resolution for the final map was determined at the 0.143 cutoff⁶.



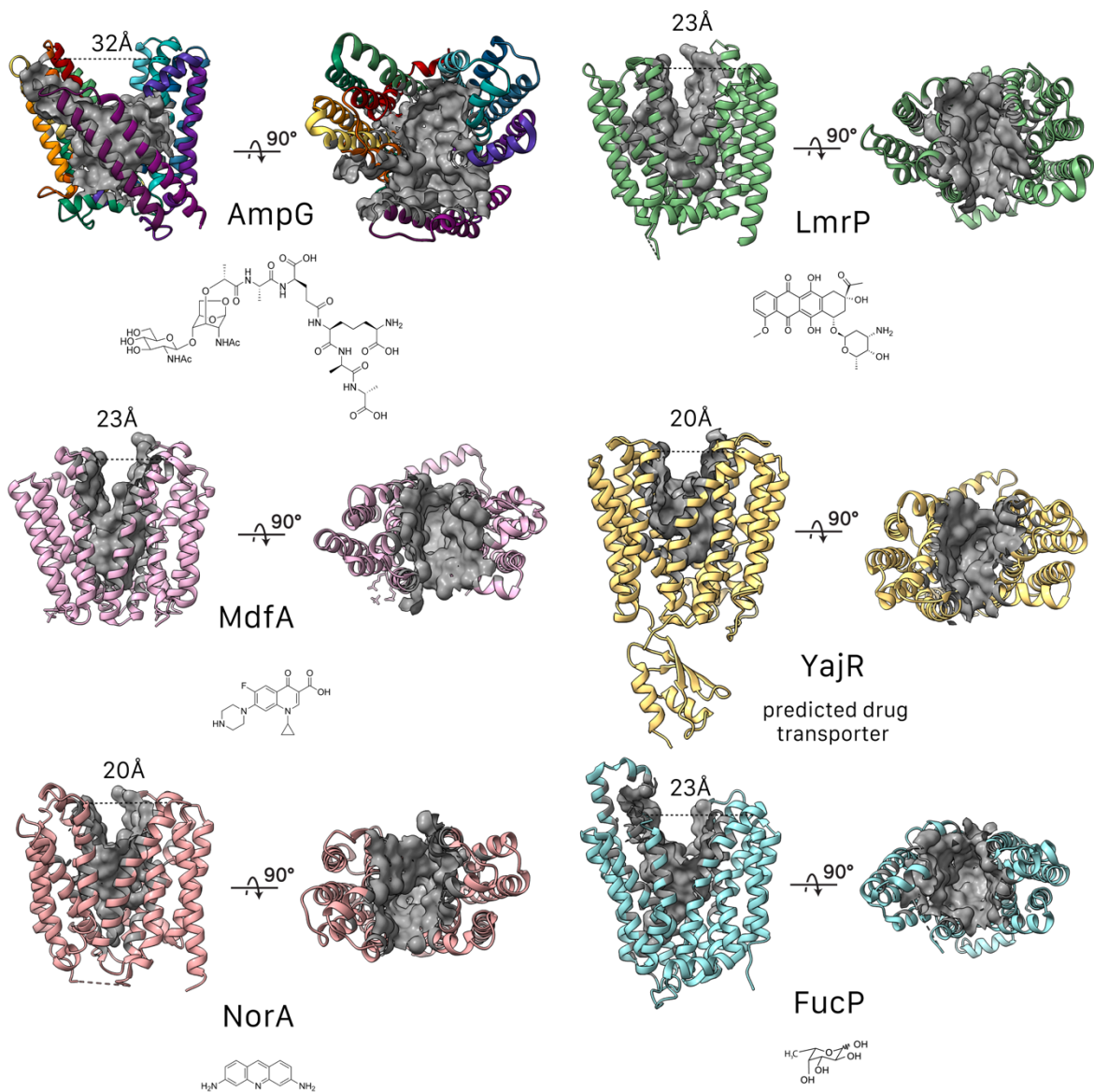
Supplementary Fig. 6: Cryo-EM sample quality. **a**, Representative micrograph of AmpG-BRIL BAG2 at 192k magnification and $-2 \mu\text{m}$ defocus. **b**, Representative 2D classes of AmpG-BRIL BAG2. BRIL and the antibody were not well resolved but helped in particle alignment. **c**, Overall reconstruction with the protein region colored according to local resolution, the diffuse detergent belt colored grey and the unresolved BRIL and BAG2 Fab purple. **d**, Density for N-terminal helices.



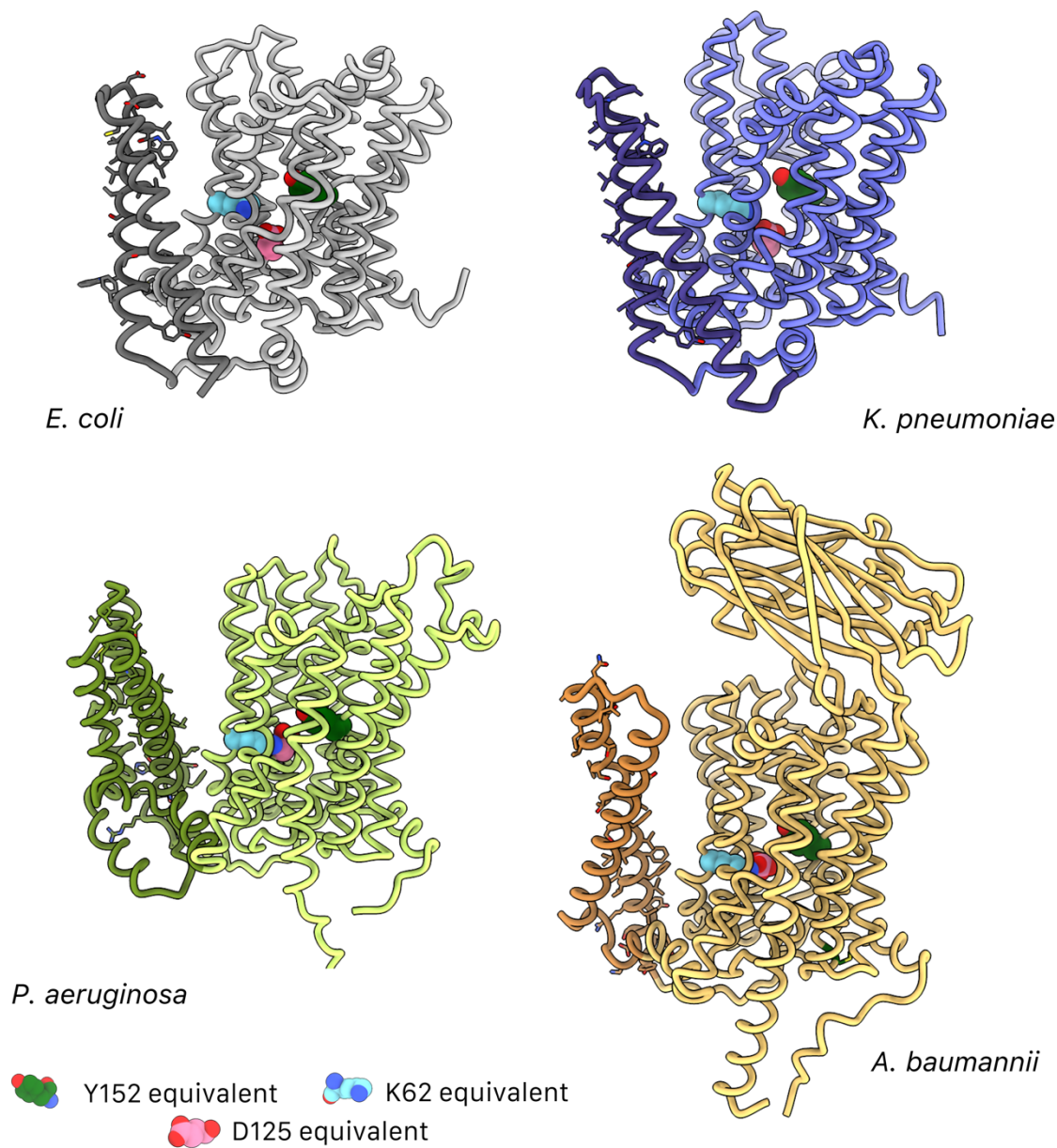
Supplementary Fig. 7. Sequence alignment of structurally related MFS transporters. *E. coli* MdfA PDB code 6GV1⁷; *L. lactis* LmrP PDB code 6T1Z⁸; *E. coli* FucP PDB code 3O7P⁹; *E. coli* YajR PDB code 3WDO¹⁰; *S. aureus* NorA PDB code 7LO8¹¹.



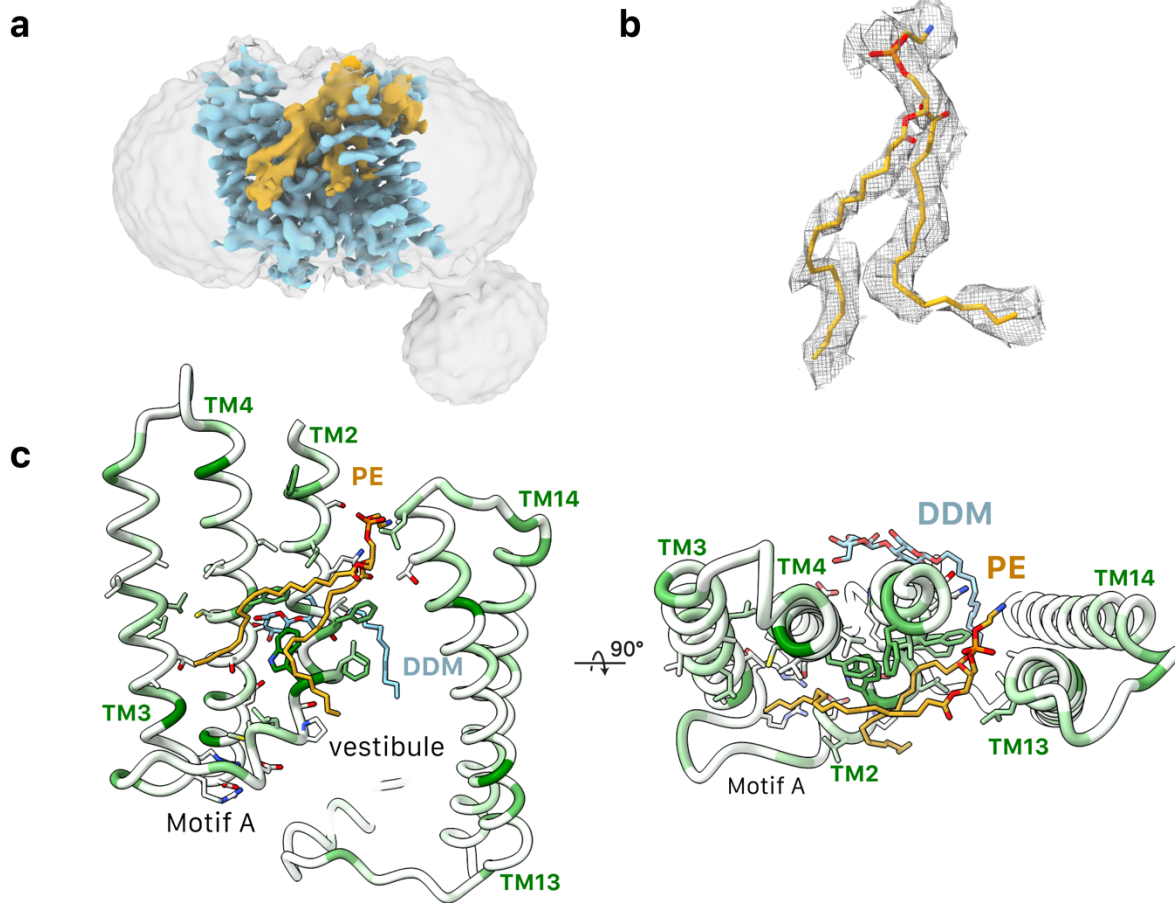
Supplementary Fig. 8: *E. coli* AmpG EVcoupling output. Evolutionary coupling analysis of AmpG sequence. Mutations in important protein interactions will influence surrounding residues, resulting in complementary mutations to preserve interactions. This analysis can use sequence evolution to accurately predict proximity in a 3D structure ¹².



Supplementary Fig. 9: Binding cavities of other structurally similar characterized MFS proteins. Surface area of structurally similar MFS protein cavities were visualized using CastP server¹³. Distances across the top cavity from the top residue C α of homologous helices compared to AmpG's TM2 and TM11. Substrates of transporters are indicated below. AmpG: GlcNAc-1,6-anhydroMurNAc-pentapeptide¹⁴; *E. coli* MfdA PDB code 6GV1⁷ fluoroquinolones, ex. Ciprofloxacin¹⁵; *S. aureus* NorA PDB code 7LO8¹¹, fluoroquinolones and acriflavine, ex. Acriflavine¹⁶; *E. coli* FucP PDB code 3O7P⁹, L-fucose; *L. lactis* LmrP PDB code 6T1Z⁸, Daunomycin, ethidium bromide, tetraphenylphosphonium, ex. Daunomycin¹⁷; *E. coli* YajR PDB code 3WDO, putative drug transporter¹⁰.



Supplementary Fig. 10: Conservation of AmpG structure in clinically relevant pathogens. Conserved key residues of the substrate binding cavity and presence of the hydrophobic vestibule formed by the insertions of added TM helices modeled in AmpG proteins from other bacterial strains. The helices making the vestibule are C-terminal sequence additions in *E. coli* and *K. pneumoniae*, but internal sequence insertions in *P. aeruginosa* and *A. baumannii*. Conserved residues involved in substrate binding shown as spheres. Models were created with AlphaFold3³.



Supplementary Fig. 11: Non-protein density in AmpG. Additional non-protein density is evident in AmpG **a**, AmpG colored blue, the detergent belt colored grey with the gold density representing the presence of detergent, lipid or possibly *E. coli* endogenous substrates that have co-purified, in the vestibule and funneling into the cavity. **b**, Density for modeled phosphatidylethanolamine (PE). Lipid in stick representation using cpk coloring with gold carbon atoms. **c**, Views of the PE binding site in the context of the C-terminal hydrophobic vestibule and MFS protein core (hydrophobic coil representation, lipid as in **b**). The PE headgroup sits on the surface of the membrane bilayer at the lateral entrance to the substrate binding cavity while the acyl tails extend across hydrophobic residues on TM2 down to motif A.

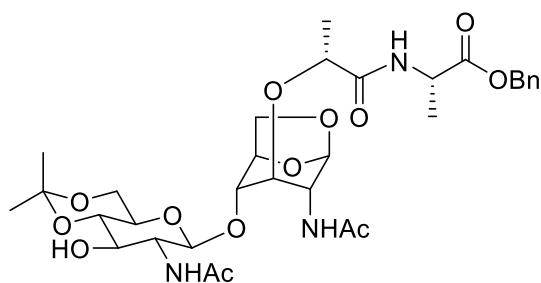
Supplementary Methods

Construct	Species	Primer Forward	Reverse
AmpG WT	<i>E.coli</i>	CCTGGTGCCGCGCGGCAGCCA TATGTCCAGTCAATATTTACG TATTTTTCAACAGC	GGATCTCAGTGGTGGTGGTGGT GGTGCTCGAGTTACGTCAGATG CGTTTTTCGTAGC
BRIL		CTTACAGGCCTGGATGACGGT CGCTGATCTTGAAGACAATTG G	CCAGAGAGAAGAAACCAATGG TTTTGAGCAGATACTTCTGGAT ATAGGC
AmpG BRIL	<i>E. coli</i>	CTTACAGGCCTGGATGACGGT CGCTGATCTTGAAGACAATTG G	CCAGAGAGAAGAAACCAATGG TTTTGAGCAGATACTTCTGGAT ATAGGC
AmpG WT	<i>P. aeruginosa</i>	ATATGGTACCATGACTCAGC AATCCTGGCGAGAGG	TAATAAGCTTGGCGAATGCCG GCCTTTTTCACTCTCG

Supplementary Table 2: Oligonucleotide primers used for cloning

Synthetic Procedures

Compound 5



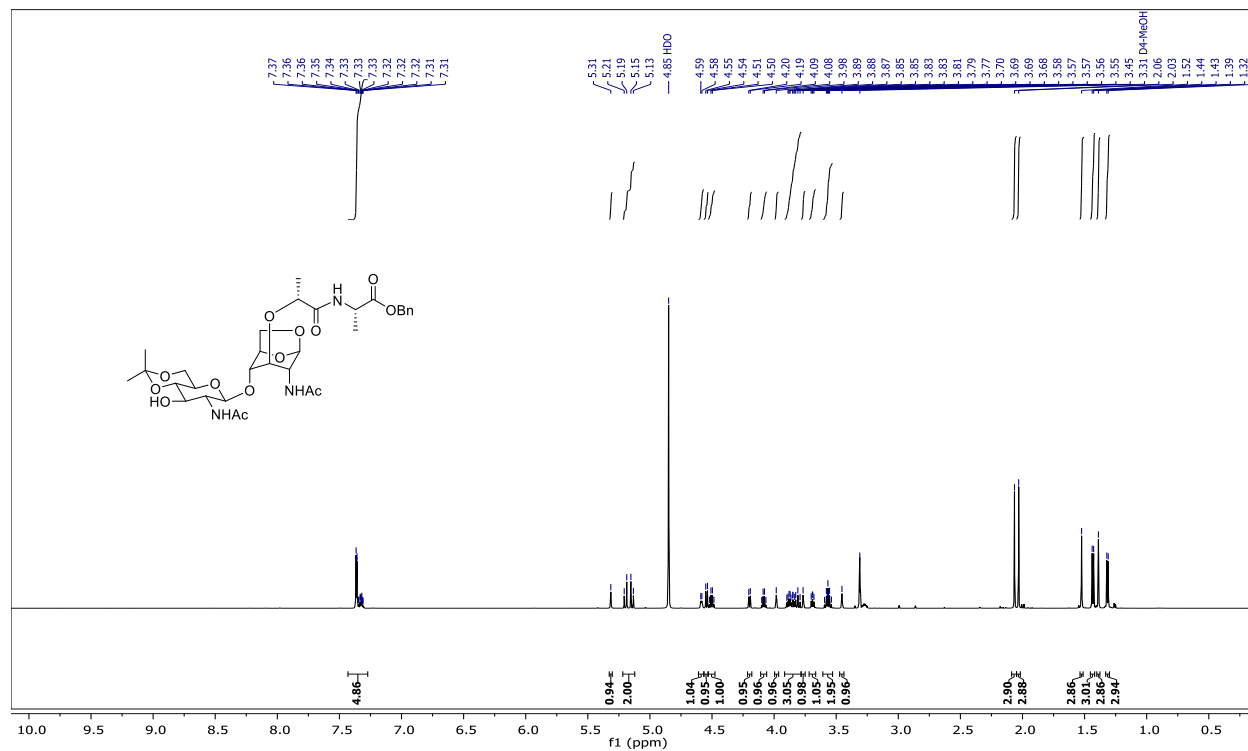
To GlcNAc-1,6-anhydroMurNAc **1** (37 mg, 0.077 mmol) was added PyBOP (66 mg, 0.13 mmol, 1.6 eq), HOBt•H₂O (23 mg, 0.15 mmol, 2 eq), L-alanine(OBn)•hydrochloride (35 mg, 0.16 mmol, 2.1 eq), and DIPEA (0.04 mL, 0.23 mmol, 3 eq) in 2 mL of degassed DMF. This solution was left to stir at rt for 40 h, after which 1 mL of H₂O and 1 mL of EtOAc was added and the solution was concentrated under reduced pressure to give an amber wax. This material was wet loaded with distilled H₂O onto a 2 g reverse-phase C₁₈ Sepack column. The column was run with step-wise gradient elution: pure distilled H₂O → 10% MeCN:90% distilled H₂O → 20% MeCN:80% distilled H₂O. The 20% MeCN fractions were concentrated to give a clear colourless wax. To this clear wax was added 1 mL of degassed DMF, 1 mL of acetone, 1 mL of 2,2-dimethoxypropane, and HOTs•H₂O (15 mg, 0.087 mmol, 1.1 eq). This solution was left to stir at rt for 24 h, after which 1 mL of EtOAc and several drops of sat aq NH₄OH were added to quench the reaction and the solution was concentrated under reduced pressure to give white precipitate. This crude product was wet purified by silica gel chromatography. The column was run with stepwise gradient elution: 5% MeOH:95% DCM → 6% MeOH:94% DCM → 7% MeOH:93% DCM. Compound **5** was attained as a white solid (23 mg, 44%).

¹H NMR (600 MHz, Methanol-*d*₄) δ 7.43 – 7.27 (m, 5H), 5.31 (s, 1H), 5.22 – 5.12 (m, 2H), 4.59 (d, *J* = 5.4 Hz, 1H), 4.54 (d, *J* = 8.4 Hz, 1H), 4.50 (q, *J* = 7.3 Hz, 1H), 4.20 (d, *J* = 7.4 Hz, 1H), 4.08 (q, *J* = 6.8 Hz, 1H), 3.98 (s, 1H), 3.92 – 3.78 (m, 3H), 3.77 (s, 1H), 3.69 (dd, *J* = 7.5, 5.7 Hz, 1H), 3.61 – 3.53 (m, 2H), 3.45 (s, 1H), 2.06 (s, 3H), 2.03 (s, 3H), 1.52 (s, 3H), 1.43 (d, *J* = 7.3 Hz, 3H), 1.39 (s, 3H), 1.32 (d, *J* = 6.8 Hz, 3H).

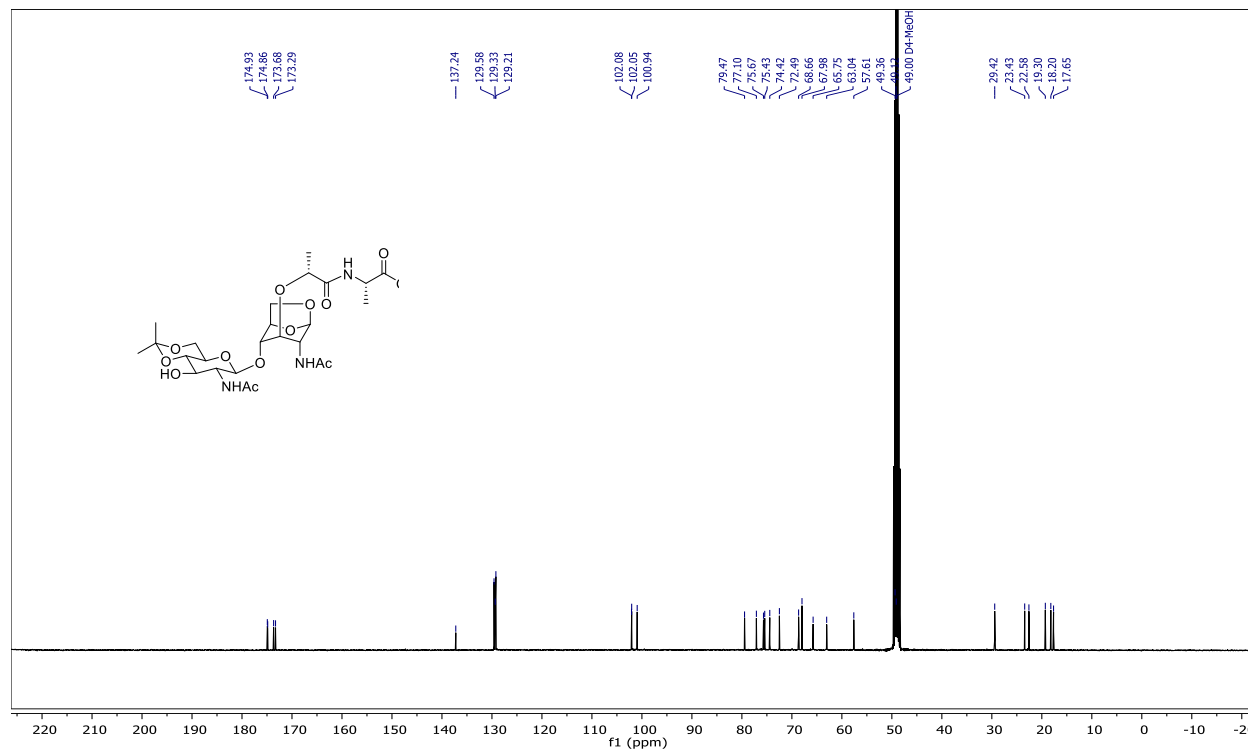
¹³C NMR (101 MHz, MeOD) δ 174.93, 174.86, 173.68, 173.29, 137.24, 129.58, 129.33, 129.21, 102.08, 102.05, 100.94, 79.47, 77.10, 75.67, 75.43, 74.42, 72.49, 68.66, 67.98, 65.75, 63.04, 57.61, 49.36, 49.12, 29.42, 23.43, 22.58, 19.30, 18.20, 17.65.

HRMS (ESI): *m/z* calc for C₃₂H₄₅N₃O₁₃ [M+Na]⁺ 702.2850, found 702.2844

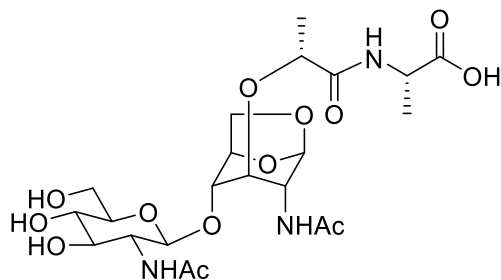
Compound 5 – ^1H NMR (Methanol- d_4 , 600 MHz)



Compound 5 – ^{13}C NMR (Methanol- d_4 , 101 MHz)



Compound 2



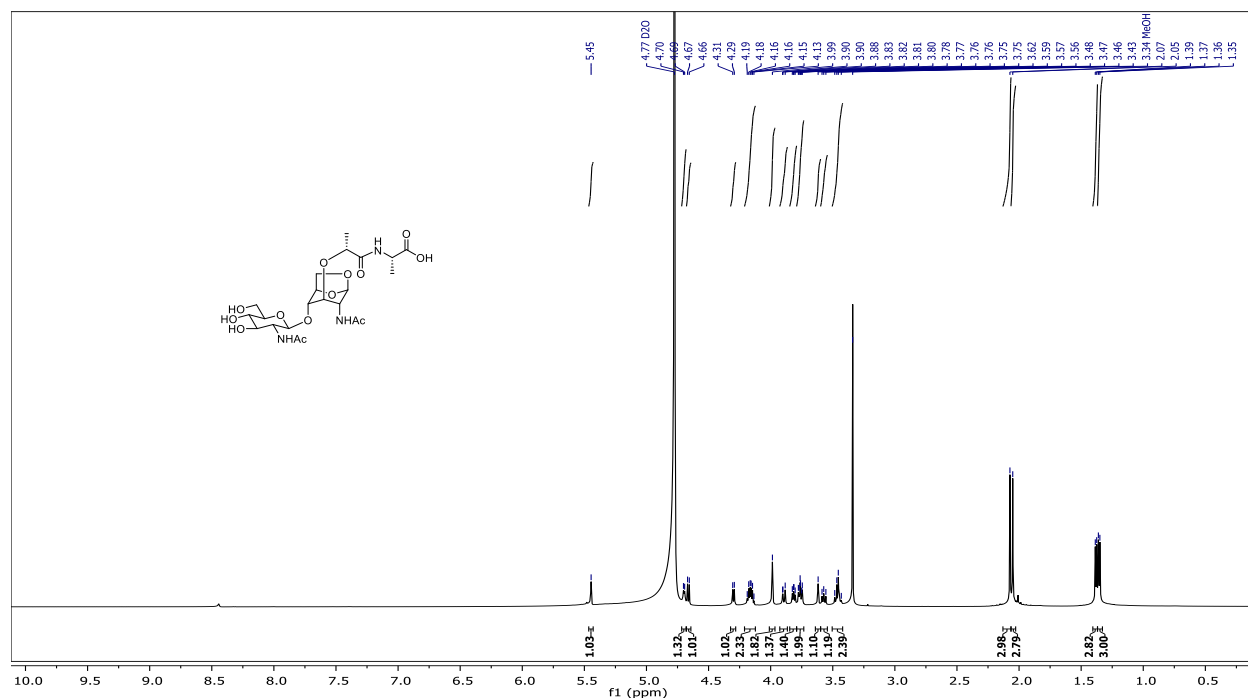
Compound **5** (13 mg, 0.019 mmol) was diluted in 3 mL of MeOH and 3 mL of H₂O and left stirring with 97 mg of 50W X8 hydrogen form Dowex resin at rt for 20 h. The solution was filtered through fritted glass via MeOH eluent and the filtrate was concentrated to give a clear colourless film. This film was redissolved in 5 mL of MeOH and 9 mg of 10% Pd/C (0.7 wt eq) was added. This solution was stirred under a H₂ atmosphere at rt for 4 h. This solution was then filtered through Celite® on top of a fine fritted glass funnel with MeOH eluent and subsequently concentrated under reduced pressure to give **2** as a clear colourless film (11 mg, quant). NMR samples were doped with MeOH as an internal standard for ¹³C NMR.

¹H NMR (600 MHz, D₂O with an internal standard of MeOH) δ 5.45 (s, 1H), 4.70 (d, *J* = 5.6 Hz, 1H), 4.66 (d, *J* = 8.4 Hz, 1H), 4.30 (d, *J* = 7.8 Hz, 1H), 4.16 (dq, *J* = 13.6, 7.0 Hz, 2H), 3.99 (s, 2H), 3.93 – 3.87 (m, 1H), 3.85 – 3.79 (m, 1H), 3.76 (td, *J* = 8.6, 3.3 Hz, 2H), 3.62 (s, 1H), 3.60 – 3.54 (m, 1H), 3.50 – 3.42 (m, 2H), 2.07 (s, 3H), 2.05 (s, 3H), 1.38 (d, *J* = 6.8 Hz, 3H), 1.36 (d, *J* = 7.2 Hz, 3H).

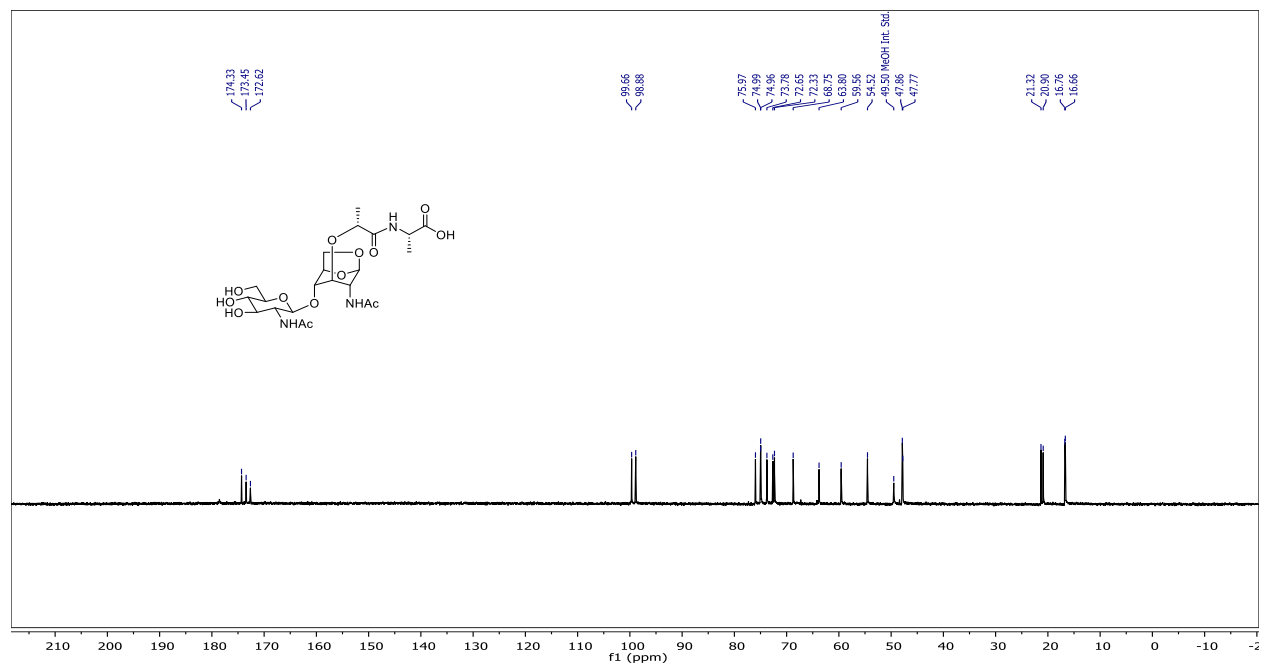
¹³C NMR (101 MHz, D₂O) δ 174.33, 173.45, 172.62, 99.66, 98.88, 75.97, 74.99, 74.96, 73.78, 72.65, 72.33, 68.75, 63.80, 59.56, 54.52, 47.86, 47.77, 21.32, 20.90, 16.76, 16.66.

HRMS (ESI): *m/z* calc for C₂₂H₃₅N₃O₁₃ [M+Na]⁺ 572.2068, found 572.2063.

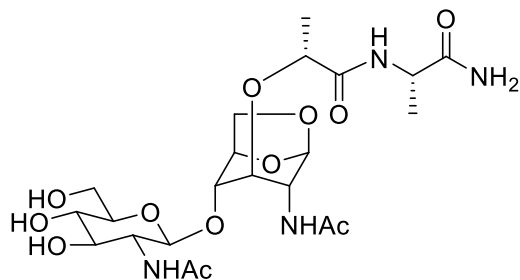
Compound 2 – ^1H NMR (D_2O with an internal standard of CH_3OH , 600 MHz)



Compound 2 – ^{13}C NMR (D_2O with an internal standard of CH_3OH , 101 MHz)



Compound 3



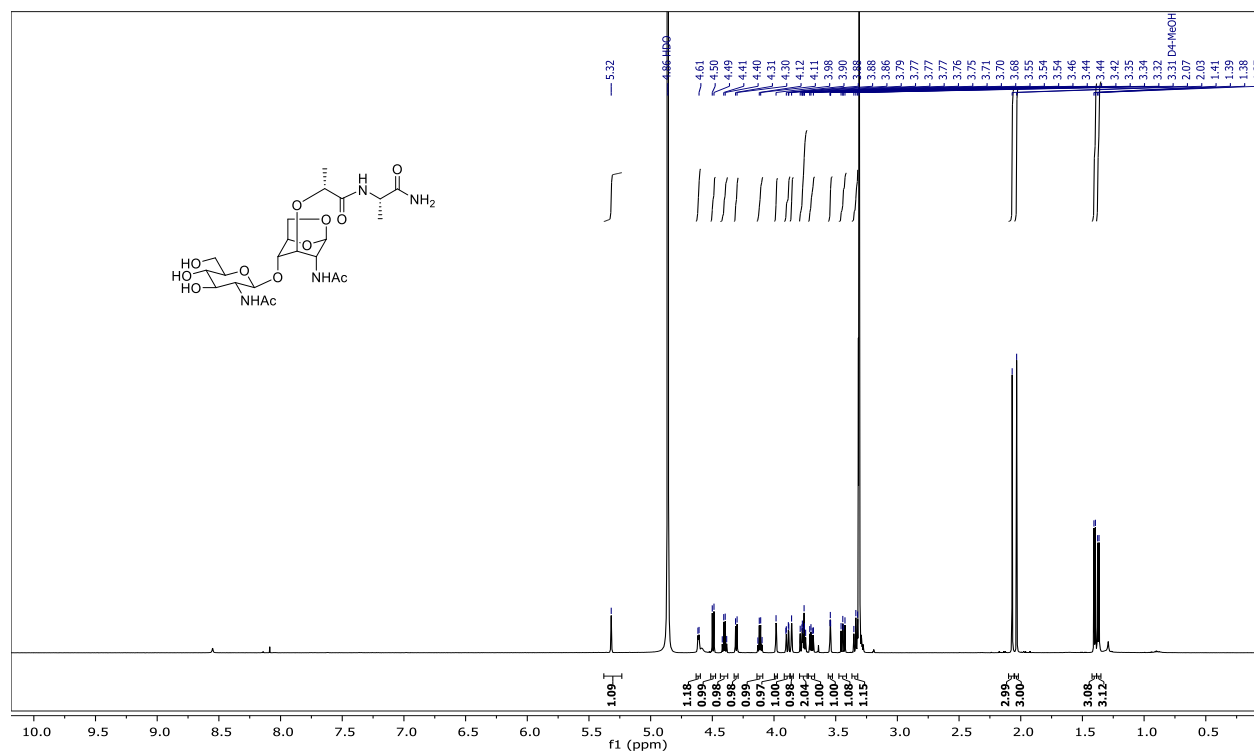
Compound **5** (11 mg, 0.016 mmol) was dissolved in 2 mL of 7M NH₃ in MeOH and left to stir at rt for 68 h. The solution was then concentrated under reduced pressure to give a clear colourless film. This film was purified by silica gel chromatography. The column was run with stepwise gradient elution: 7% MeOH:93% DCM → 8% MeOH:92% DCM. The acetonide-protected primary amide intermediate was attained as a white solid. This solid was diluted in 2 mL of MeOH and 2 mL of H₂O and left stirring with 85 mg of 50W X8 hydrogen form Dowex resin at rt for 20 h. The solution was filtered through fritted glass via MeOH eluent and the filtrate was concentrated to give **3** as a clear colourless film (7.5 mg, 85% yield).

¹H NMR (600 MHz, Methanol-*d*₄) δ 5.32 (s, 1H), 4.61 (d, *J* = 5.4 Hz, 1H), 4.49 (d, *J* = 8.4 Hz, 1H), 4.40 (q, *J* = 7.1 Hz, 1H), 4.31 (d, *J* = 7.5 Hz, 1H), 4.11 (q, *J* = 6.8 Hz, 1H), 3.98 (s, 1H), 3.89 (dd, *J* = 11.9, 2.2 Hz, 1H), 3.86 (s, 1H), 3.79 – 3.73 (m, 2H), 3.70 (dd, *J* = 11.9, 5.8 Hz, 1H), 3.56 – 3.53 (m, 1H), 3.44 (dd, *J* = 10.5, 8.5 Hz, 1H), 3.37 – 3.32 (m, 1H), 2.07 (s, 3H), 2.03 (s, 3H), 1.40 (d, *J* = 7.1 Hz, 3H), 1.37 (d, *J* = 6.8 Hz, 3H).

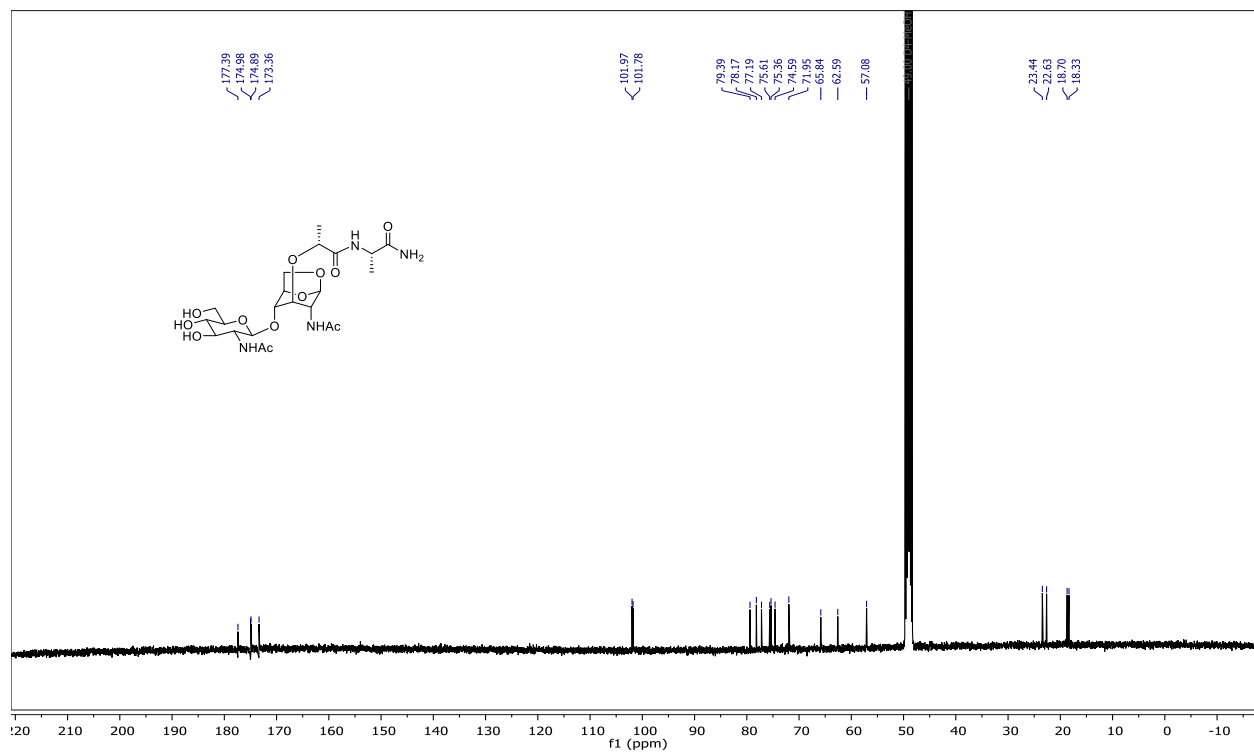
¹³C NMR (101 MHz, MeOD) δ 177.39, 174.98, 174.89, 173.36, 101.97, 101.78, 79.39, 78.17, 77.19, 75.61, 75.36, 74.59, 71.95, 65.84, 62.59, 57.08, 23.44, 22.63, 18.70, 18.33.

HRMS (ESI): *m/z* calc for C₂₂H₃₆N₄O₁₂ [M+Na]⁺ 571.2231, found 571.2225.

Compound 3 - ^1H NMR (Methanol- d_4 , 600 MHz)



Compound 3 - ^{13}C NMR (Methanol- d_4 , 101 MHz)



References

1. Robert, X. & Gouet, P. (2014) 'Deciphering key features in protein structures with the new ENDscript server'. *Nucl. Acids Res.* 42(W1), W320-W324 - doi: 10.1093/nar/gku316 (freely accessible online).
2. Sayers, E. W. *et al.* Database resources of the National Center for Biotechnology Information. *Nucleic Acids Res.* **50**, D20–D26 (2021).
3. Abramson, J. *et al.* Accurate structure prediction of biomolecular interactions with AlphaFold 3. *Nature* 1–3 (2024) doi:10.1038/s41586-024-07487-w.
4. Bayburt, T. H. & Sligar, S. G. Membrane protein assembly into Nanodiscs. *FEBS Lett.* **584**, 1721–1727 (2010).
5. Punjani, A., Rubinstein, J. L., Fleet, D. J. & Brubaker, M. A. cryoSPARC: algorithms for rapid unsupervised cryo-EM structure determination. *Nat. Methods* **14**, 290–296 (2017).
6. Rosenthal, P. B. & Henderson, R. Optimal Determination of Particle Orientation, Absolute Hand, and Contrast Loss in Single-particle Electron Cryomicroscopy. *J. Mol. Biol.* **333**, 721–745 (2003).
7. Eisinger, M. L., Dörrbaum, A. R., Michel, H., Padan, E. & Langer, J. D. Ligand-induced conformational dynamics of the Escherichia coli Na⁺/H⁺ antiporter NhaA revealed by hydrogen/deuterium exchange mass spectrometry. *Proc. Natl. Acad. Sci.* **114**, 11691–11696 (2017).
8. Debruycker, V. *et al.* An embedded lipid in the multidrug transporter LmrP suggests a mechanism for polyspecificity. *Nat. Struct. Mol. Biol.* **27**, 829–835 (2020).
9. Dang, S. *et al.* Structure of a fucose transporter in an outward-open conformation. *Nature* **467**, 734–738 (2010).
10. Jiang, D. *et al.* Structure of the YajR transporter suggests a transport mechanism based on the conserved motif A. *Proc. Natl. Acad. Sci.* **110**, 14664–14669 (2013).
11. Brawley, D. N. *et al.* Structural basis for inhibition of the drug efflux pump NorA from *Staphylococcus aureus*. *Nat. Chem. Biol.* **18**, 706–712 (2022).
12. Nicoludis, J. M. & Gaudet, R. Applications of sequence coevolution in membrane protein biochemistry. *Biochim. Biophys. Acta* **1860**, 895–908 (2018).
13. Ye, B., Tian, W., Wang, B. & Liang, J. CASTpFold: Computed Atlas of Surface Topography of the universe of protein Folds. *Nucleic Acids Res.* gkae415 (2024) doi:10.1093/nar/gkae415.
14. Cheng, Q. & Park, J. T. Substrate specificity of the AmpG permease required for recycling of cell wall anhydro-muropeptides. *J. Bacteriol.* **184**, 6434–6436 (2002).
15. Wu, H.-H., Symersky, J. & Lu, M. Structure of an engineered multidrug transporter MdfA reveals the molecular basis for substrate recognition. *Commun. Biol.* **2**, 1–12 (2019).
16. Yu, J.-L., Grinius, L. & Hooper, D. C. NorA Functions as a Multidrug Efflux Protein in both Cytoplasmic Membrane Vesicles and Reconstituted Proteoliposomes. *J. Bacteriol.* **184**, 1370–1377 (2002).
17. Roth, A. & Govaerts, C. LmrP from *Lactococcus lactis*: a tractable model to understand secondary multidrug transport in MFS. *Res. Microbiol.* **169**, 468–477 (2018).